Chemical Science

ROYAL SOCIETY OF CHEMISTRY

EDGE ARTICLE

View Article Online
View Journal | View Issue

Check for updates

Cite this: *Chem. Sci.*, 2025, **16**, 3888

All publication charges for this article have been paid for by the Royal Society of Chemistry

Received 24th November 2024
Accepted 15th January 2025

DOI: 10.1039/d4sc07938h

rsc.li/chemical-science

Open Access Article. Published on 22 2568. Downloaded on 10/8/2568 14:13:08.
This article is licensed under a Creative Commons Attribution 3.0 Unported Licence.

Metal–ligand cooperativity enables zero-valent metal transfer†

Martin-Louis Y. Riu, Jing-Ran Shan, K. N. Houk * and Matthew Nava *

Group 13 aminoxy complexes of the form (L)E(TEMPO)$_3$ (TEMPO = 2,2,6,6-tetramethylpiperidine 1-oxyl; L = THF (tetrahydrofuran) or Py (pyridine); E = Al, Ga, In) were prepared and structurally characterized. The complexes (THF)Ga(TEMPO)$_3$ (**1**·THF) and (Py)In(TEMPO)$_3$ (**2**·Py) are shown to heterolytically cleave H_2 under mild conditions (3 atm, 20 °C, $t \leq 1$ h). **1**·THF reacts reversibly with H_2 to form a formal H_2-adduct that bears a Ga(III) hydride site and a protonated TEMPO ligand with concomitant loss of THF, consistent with Ga(III) and TEMPO functioning as Lewis acid and base, respectively. Conversely, **2**·Py is reduced by H_2 to form an intermediate dimer complex of monovalent {In(TEMPO)}$_2$, which undergoes further reactivity with H_2 to form elemental indium as determined by powder X-ray diffraction. Treatment of **2**·Py with H_2 and Ph_3PSe forms binary InSe, in addition to Ph_3P and TEMPOH, demonstrating that **2**·Py functions as a molecular source of zero-valent indium under mildly reducing conditions. Computational studies support an intramolecular metal–ligand cooperativity pathway in the heterolytic cleavage of H_2.

Introduction

Metal–ligand cooperativity (MLC), which describes the synergistic interaction of metal and ligand with substrate in bond forming or breaking events, is a well-established tool in transition metal-mediated bond activation and catalysis[1] and commonly found in nature.[2] While this concept may be applied generally and used to impart redox innocent metals with ambiphilic properties, the field of MLC based on the p-block elements is considerably less developed.[3] This approach complements existing major strategies in the burgeoning field of bond activation and catalysis by the p-block elements[4,5] which rely on steric[6] or geometric[7,8] frustration or the generation of low-valent element sites;[9,10] though we should note that parallels between MLC and frustrated Lewis pair (FLP) chemistry have been previously identified and the line distinguishing the two fields is often blurred.[11]

With the aim of imparting ambiphilicity on complexes of redox innocent trivalent group 13 metals, we have identified TEMPO (2,2,6,6-tetramethylpiperidine 1-oxyl) as a suitable ligand that may facilitate the heterolytic cleavage of H_2 through MLC. In fact, tripodal tris(aminoxy)-supported group 13 complexes were recently shown to reversibly react with O–H bonds through a MLC pathway.[12] Herein, we describe our initial investigation that revealed examples of remarkably facile dihydrogen activation. For indium, this process led to zero-valent metal generation, and when repeated in the presence of a selenium source, binary InSe was obtained, consistent with TEMPO functioning as a facilitative and removable ligand following H_2 activation. Canonically, MLC has been leveraged for the activation of small molecules and in select cases catalysis, but to our knowledge the engineering of MLC to facilitate the preparation of materials is rare.

Results and discussion

Group 13-aminoxy complexes, in analogy to homoleptic first row TM complexes,[13] were prepared *via* salt metathesis reactions of ECl_3 (E = Ga, In, Al) and NaTEMPO (3 equiv.) in tetrahydrofuran (THF), leading to **1**·THF, **2**·THF, and **3**·THF (Fig. 1A). The complexes were isolated in 60%, 38%, and 55% yield (**1**·THF, **2**·THF, and **3**·THF, respectively) following crystallization. Single crystal X-ray diffraction (SC-XRD) experiments revealed nearly trigonal monopyramidal geometries with THF occupying the apical position of the complexes, consistent with the significant steric bulk of the aminoxy ligands (Fig. 1B; see S.2†). The SC-XRD experiments also revealed average (avg.) N–O bond lengths (Table 1) that are similar to those of related dialkylaminoxy group 13 complexes and relatively short M–O(TEMPO) bond lengths.[14–19] Reflecting the sterically congested geometries, longer than expected metal-THF bond lengths were observed (In: 2.251(10) Å, Ga: 2.0518(11) Å, Al: 1.9130(17) Å; Table 1).[20,21] Dissolution of the complexes in pyridine-d_5 results in the corresponding pyridine adducts and free THF, suggesting rapid ligand exchange at room temperature and is consistent with the greater basicity of pyridine. Heating the complexes in a poorly coordinating solvent (benzene-d_6, 80 °C) leads to

Department of Chemistry and Biochemistry, University of California, Los Angeles, California 90095-1569, USA. E-mail: mnava@chem.ucla.edu; houk@chem.ucla.edu

† Electronic supplementary information (ESI) available. CCDC 2347342–2347346. For ESI and crystallographic data in CIF or other electronic format see DOI: https://doi.org/10.1039/d4sc07938h

© 2025 The Author(s). Published by the Royal Society of Chemistry

Open Access Article. Published on 22 2568. Downloaded on 10/8/2568 14:13:08.
This article is licensed under a Creative Commons Attribution 3.0 Unported Licence.

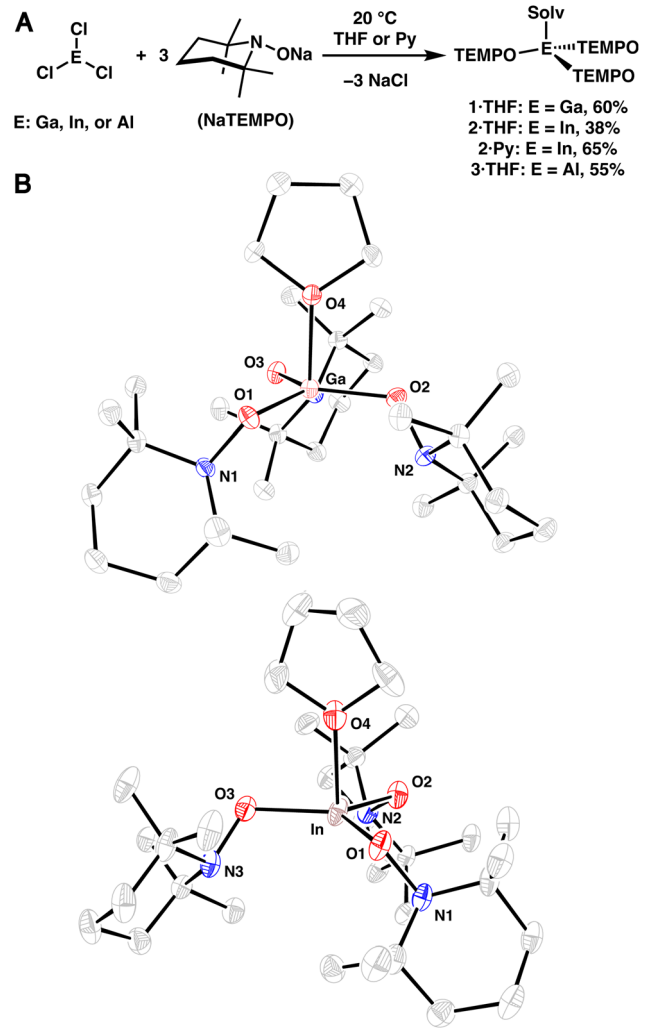

Fig. 1 (A) Synthesis of aminoxy complexes **1**·THF, **2**·THF, **2**·Py, and **3**·THF. (B) SC-XRD structure of **1**·THF (top) and **2**·THF (bottom) with thermal ellipsoids shown at the 50% probability level. Hydrogen atoms are omitted for clarity.

Table 1 Table of selected bond lengths (Å) determined *via* SC-XRD experiments (average, avg.)

Complex	M–THF	M–O(TEMPO) (avg.)	N–O (avg.)
3·THF	1.9130(17)	1.74	1.45
1·THF	2.0518(11)	1.82	1.46
2·THF	2.251(10)	2.01	1.46

complex mixtures within 1 h (see S.1.6†), indicating that coordination of solvent is crucial to the stability of the complexes. Complex **2**·THF exhibits particularly poor stability in non-donor solvents; therefore, the corresponding pyridine adduct **2**·Py was prepared and isolated independently in an improved yield of 65% (Fig. 1A).

Recognizing the potentially ambiphilic nature of the complexes described above, where the metal atom and TEMPO ligand function as a Lewis acid and base, respectively, reactions with dihydrogen were investigated. Treatment of **1**·THF in *n*-hexane (0.02 M) with H_2 (3 atm) results in complete conversion to **4** at 20 °C within 1 h, which was isolated *via* crystallization in 62% yield (Fig. 2A). Consistent with our assignment, ^{1}H NMR spectroscopic analysis of the crude reaction mixture in benzene-d_6 revealed a broad ($\omega_{1/2}$ = 45 Hz) singlet at 5.72 ppm, diagnostic of a terminal Ga–H resonance,[22] and a deshielded resonance at 8.88 ppm, which corresponds to Ga-bound N-protonated TEMPO ligand.[23] Additionally, infrared (IR) spectroscopy of this mixture revealed bands at 1930 and 3570 cm^{-1}, which correspond to the Ga–H and N–H stretches, respectively.[22,23] Furthermore, the structure of **4** was confirmed in a SC-XRD experiment (Fig. 2B). The overall neutral charge of **4** indicates that H_2 is split heterolytically, resulting in the formation of a protonated amine (H^+) and a gallium hydride (H^-). In contrast to the relatively small (THF)–Ga–O(TEMPO) average bond angle of 95.3° observed in **1**·THF, complex **4** exhibits an average H–Ga–O(TEMPO) bond angle of 113.6°, consistent with a strong hydride adduct. Additionally, the Ga–O1 bond length in **4** is 1.9407(14) Å, which is relatively long when compared to that of Ga–O2 and Ga–O3 (1.8404(13) Å and 1.8634(13) Å, respectively), reflecting protonation of N1 in the complex. An intramolecular hydrogen-bonding interaction is also likely present in complex **4**, with the O3–H2 interatomic distance measuring 2.038(25) Å.

To confirm the origin of the newly installed hydrogen atoms, a deuterium labeling experiment was performed using D_2 in place of H_2 which resulted in the disappearance of the N–H and Ga–H resonances and vibrational bands in the ^{1}H NMR and IR spectra, respectively (see S.1.8.2†). While we were able to confirm isotopic substitution *via* ^{2}H NMR spectroscopy, we were unable to observe the Ga–D and N–D vibrational modes possibly due to overlapping solvent. The thermal stability of **4** in pyridine-d_5 was also investigated (see S.1.9†), and we observed free H_2 and the partial formation of **1**·Py by ^{1}H NMR spectroscopy

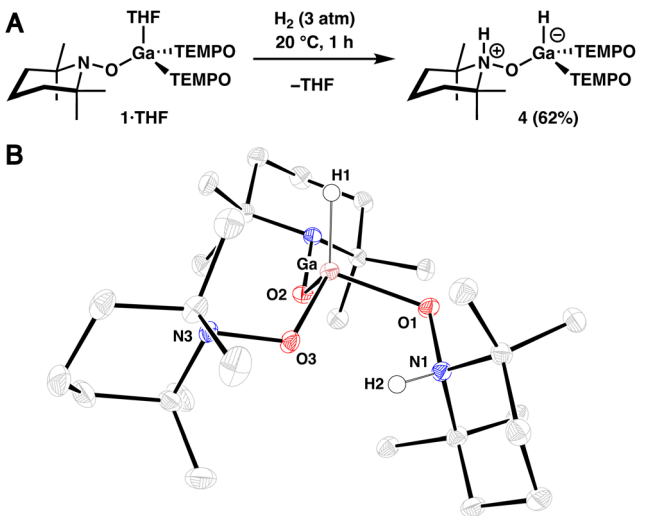

Fig. 2 (A) Synthesis of dihydrogen adduct **4**. (B) SC-XRD structure of **4** with thermal ellipsoids shown at the 50% probability level. Selected hydrogen atoms are omitted for clarity.

Open Access Article. Published on 22 2568. Downloaded on 10/8/2568 14:13:08.
This article is licensed under a Creative Commons Attribution 3.0 Unported Licence.

after heating a solution of **4** to 80 °C for 20 h, indicating that **1** is able to reversibly bind H_2.

For context, Aldridge reported H_2 activation by an ambiphilic Ga^{III} complex, which was supported by an appreciably basic β-diketiminato (Nacnac)-derived dianionic diamide ligand framework, under albeit more forcing conditions (4 atm, 70 °C, 12 h).[24,25] Goicoechea reported the facile activation of H_2 by a phosphine-substituted phosphagallene,[26,27] while Mitzel has developed an Al–O–P system,[28] both of which similarly function as single-component FLPs. Additionally, the heterolytic cleavage of H_2 under mild conditions was also observed for intermolecular FLPs based on P^tBu_3 and potent Lewis acids $E(C_6F_5)_3$ (E = Ga or In), leading to a E–H–E bridging hydride.[29] Notably, none of the Ga-based systems above are reported to reversibly bind H_2.

Similar to **1**·THF, **2**·Py readily activates H_2. However, treatment of **2**·Py in *n*-hexane (0.03 M) with H_2 (3 atm) at 20 °C results in free TEMPOH and the In^I complex **5** in a 2 : 1 ratio within 1 h as assessed by NMR spectroscopy (Fig. 3A). The reaction of **2**·Py with H_2 appears to be tolerable of donor solvents and cleanly provides TEMPOH and **5** when combined in pyridine-d_5 (see S.1.10.4†). Complex **1**·THF, on the other-hand, reacts sluggishly with H_2 in pyridine-d_5 (see S.1.8.4†), possibly indicating the presence of a free coordination site plays a more important role in the latter complex. Complex **5** was isolated as a yellow, crystalline material in 65% yield and its identity was confirmed by SC-XRD (Fig. 3B). We propose that monovalent **5** forms *via* H_2 reductive elimination following two sequential H_2 activation reactions with **2** and subsequent dissociation of two TEMPOH ligands (see Section S.3.1.2† for a more detailed discussion on the potential mechanism). Note that reductive loss of H_2 following H_2 activation and subsequent dissociation of TEMPOH is expected given the high lability of In–H bonds in the absence of a stabilizing ligand environment.[30–32] When the reaction was repeated with D_2 in place of H_2, a new band at 2634 cm^{-1} corresponding to the O–D stretch of free TEMPOD was observed (Fig. S.48†), matching previously reported data.[33] To the best of our knowledge, the demonstration of H_2 activation by an In complex under mild conditions is unprecedented.[29]

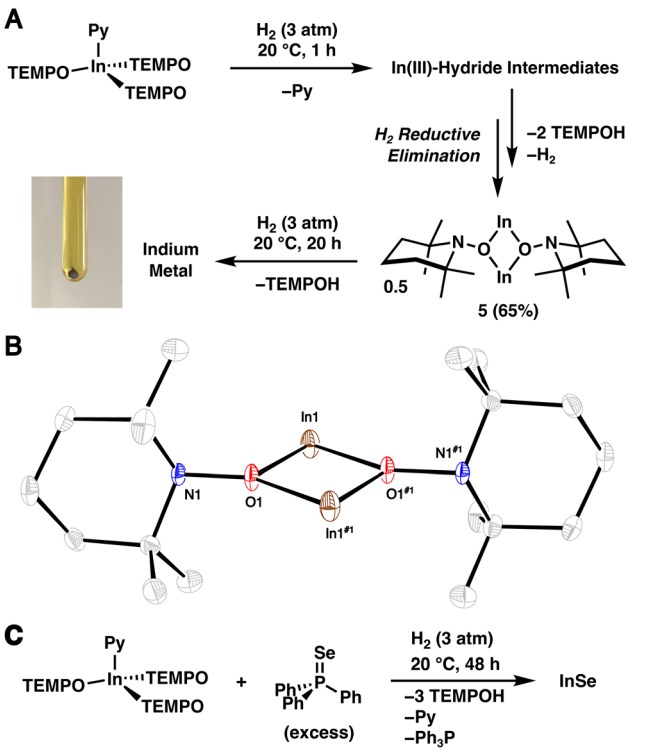

Fig. 3 (A) Treatment of **2**·Py with H_2 leading to **5**, *via* trivalent indium hydride intermediates, and its reduction to In metal (photograph of generated In metal shown to the bottom left). (B) SC-XRD structure of **5** with thermal ellipsoids shown at the 50% probability level. Hydrogen atoms are omitted for clarity. (C) Formation of InSe from **2**·Py and Ph_3PSe.

Complex **5** exhibits N1–O1–In1 and N1–O1–$In1^{\#1}$ angles of 107.34(14)° and 143.84(15)°, respectively, suggesting a weak interaction between N1 and In1. This interaction resembles the intramolecular nitrogen–silicon donor–acceptor interactions observed in aminoxy-substituted trifluoromethylsilanes $F_3SiONMe_2$ and $(F_3C)F_2SiONMe_2$.[34,35] Additionally, the interatomic distance of 2.9670(22) Å between In1 and N1 is shorter than the sum of the van der Waals radii (4.09 Å);[36] though, we should note the limitations associated with identifying non-covalent interactions based on van der Waals radii.[37]

Extending the reaction time between **2**·Py and H_2 to 24 h leads to a gray-brown suspension. Remarkably, powder X-ray diffraction (PXRD) of the isolated solids revealed that they correspond to elemental In (Fig. S.54†),[38] suggesting that **5** reacts further with H_2 to form TEMPOH and In metal. To verify this transformation, a benzene-d_6 solution of isolated **5** was treated with H_2 (3 atm), and clean conversion to TEMPOH was observed within 20 h as assessed by ^1H NMR spectroscopy (see S.1.11†). Gray solids were also generated and confirmed to correspond to In metal by PXRD. The complete reduction of **2** to elemental In is in line with its relatively low standard aqueous reduction potential (−0.34 V *vs.* SHE for $In^{III} \rightleftharpoons In^0$).[39] When the treatment of **2**·Py with H_2 was repeated with Ph_3PSe (1.5 equiv.), orange solids corresponding to binary InSe[40] precipitated from solution within minutes, revealing that **2**·Py functions as a molecular synthon of elemental In when treated with H_2 (Fig. 3C). Notably, in a separate experiment, no reaction is observed between In powder and Ph_3PSe. Although PXRD analysis suggests the as prepared InSe is amorphous, inductively coupled plasma mass spectrometry (ICP-MS) indicates an approximate 1 : 1 In to Se stoichiometry. Consistent with aminoxy-assisted reduction, NMR analysis of the crude reaction mixture revealed TEMPOH and Ph_3P. InSe is on the binary indium–selenium phase diagram[41] and may be prepared from heating elemental indium and selenium to 900 °C[42] or electrodeposition from solutions containing indium and selenite salts.[43] The structure of the β form is known and contains an In–In bond, hence the divalent indium oxidation state.[40] Note that our sample of InSe is amorphous likely due to the very low temperature of synthesis.

To gain further insight into the discrete steps that may take place in this transformation, **5** was combined with Ph_3PSe in the absence of H_2 (Fig. 4; see S.1.18†). Within several minutes,

© 2025 The Author(s). Published by the Royal Society of Chemistry

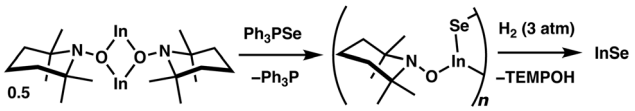

Fig. 4 Generation of a proposed oligomeric intermediate following selenium transfer from Ph_3PSe to **5** followed by the removal of the TEMPO ligands *via* the addition of H_2.

Open Access Article. Published on 22 2568. Downloaded on 10/8/2568 14:13:08.
This article is licensed under a Creative Commons Attribution 3.0 Unported Licence.

the reaction mixture became intensely yellow and remained homogeneous, and $^{31}P\{^1H\}$ NMR analysis revealed the complete conversion of Ph_3PSe to Ph_3P. Notably, broad resonances were observed in the ^1H NMR spectrum and may be attributable to an oligomeric TEMPO-substituted indium selenide intermediate (Fig. 4). Treatment of this crude reaction mixture with H_2 (3 atm) led to the precipitation of an orange solid that is consistent with InSe within minutes. Additionally, clean formation of TEMPOH was also observed indicating that the intermediate generated upon Se transfer also participates in MLC-promoted H_2 activation en route to the binary material.

Examples of molecular In complex reduction using H_2 under mild conditions are exceedingly rare, highlighting the possible utility of ligand-assisted methods of depositing and transferring zero-valent metals. Moreover, the observed reduction of phosphorus in Ph_3PSe opens the possibility of using alternative non-canonical chalcogenide sources for the preparation of materials. Our preparation brings to mind the synthesis of amorphous GaAs *via* the alcoholysis of molecular precursor $(C_5Me_5)_2Ga–As(SiMe_3)_2$; although, we should note that the formal reduction of the metal atom is not observed during the course of this reaction and the significant driving force of Si–O bond formation.[44]

Activation of H_2 by **3**·THF was also investigated; however, no reaction with H_2 (8 atm, 48 h) was observed after workup of the reaction mixture. We suspect that the greater electropositivity of Al leads to a more tightly bound metal–THF adduct and a weaker metal–hydride bond which result in thermodynamically unfavorable H_2 activation. Consequently, the relative Lewis acidities of the aminoxy complexes were determined using the Gutmann–Beckett method with Et_3PO as the Lewis base.[45] The study suggests that **3**, followed by **1** and then **2**, is the most Lewis acidic, and the observed trend is supported by computed fluoride ion affinities (FIA, Table 2). Hydride ion affinities (HIA), which better represents soft interactions due to the greater polarizability of hydride, were also computed for the aminoxy complexes.[48] This study revealed an opposing trend, where **2**, followed by **1** and **3**, exhibits the greatest HIA (Table 2). For comparison, Table 2 provides Gutmann–Beckett, FIA, and HIA values for pentafluorophenyl-substituted Lewis acids known to readily activate H_2 when combined with an external Lewis base,[29,49,50] highlighting the attenuated Lewis acidities of the aminoxy complexes presented in this work.

Density functional theory (DFT) calculations were performed to investigate the mechanism of dihydrogen activation using **1**·THF as the model substrate (Fig. 5A). The reaction initiates by dissociation of THF, leading to three-coordinate C_{3h} symmetric **IN1**. While it's unlikely that dissociation of THF from **1**·THF and **2**·THF is exergonic, the calculations ultimately suggest that dissociation of THF is nearly thermoneutral. This is consistent with the poor stabilities of complexes **1**·THF, **2**·THF, and **3**·THF in non-donor solvents and the rapid displacement of the THF ligand by pyridine, as described earlier. The subsequent formation of van der Waals complex **IN2** is slightly endergonic by 2.7 kcal mol^{-1} due to the entropic cost and is followed by the cleavage of H–H bond *via* **TS1** with a calculated activation barrier of 10.7 kcal mol^{-1}. This cooperative interaction of a hydride and proton acceptor bears a qualitative resemblance to diphosphine molecular catalysts bearing pendant amines.[51] **TS1** is followed by **IN3** (**4** when M = Ga), which is downhill by −8.3 kcal mol^{-1} as compared to **1**·THF. The activation barrier for the reverse pathway was found to be 17.7 kcal mol^{-1}, consistent with reversible dihydrogen activation observed for **1**·THF when paired with strongly coordinating pyridine.

In **TS1** (M = Ga; Fig. 5A), the H–H bond length is 0.77 Å, nearly identical to that of free dihydrogen (0.76 Å, calculated at the same level of theory) and the gallium atom retains its trigonal planar geometry. These observations indicate that **TS1** is an early transition state, structurally and energetically similar to dihydrogen adduct **IN2**. To gain further insight into the dihydrogen activation process, the forward intrinsic reaction coordinate (IRC) was calculated from **TS1** to **IN3** (Fig. 5B). A shoulder area was first observed in the IRC curves, implying large molecular and electronic structural changes in the course of reaction. Further examination into the IRC reveals that the reaction is comprised of two stages. Initially, the dihydrogen molecule approaches the reaction site without significant

Table 2 Assessment of Lewis acidity using the Gutmann–Beckett method and computed FIA and HIA for **1**, **2**, **3**, and selected Lewis acids (DSD-BLYP-D3BJ/def2-QZVPP//PBEh-3c/def2-mSVP). $\Delta\delta_{31P}$ corresponds to the $^{31}P\{^1H\}$ NMR shift of free triethylphosphine oxide (TEPO) subtracted from that of the TEPO-Lewis acid adduct

Lewis acid	$\Delta\delta_{31P}$[a] (ppm)	$\Delta\delta_{31P}$[b] (ppm)	FIA[c] (kJ mol^{-1})	HIA[d] (kJ mol^{-1})
1, $Ga(TEMPO)_3$	20.1	16.7	−353	−355
2, $In(TEMPO)_3$	18.3	14.9	−341	−374
3, $Al(TEMPO)_3$	21.1	17.4	−415	−327
$B(C_6F_5)_3$	29.7 (ref. 46)	27.0 (ref. 47)	−442	−478
$Al(C_6F_5)_3$		26.0	−549	−475
$Ga(C_6F_5)_3$		23.1	−451	−467
$In(C_6F_5)_3$		19.4	−420	−459

[a] In C_6D_6 at 25 °C. [b] In CH_2Cl_2 at 25 °C. [c] Fluoride ion affinity. [d] Hydride ion affinity.

Open Access Article. Published on 22 2568. Downloaded on 10/8/2568 14:13:08.
This article is licensed under a Creative Commons Attribution 3.0 Unported Licence.

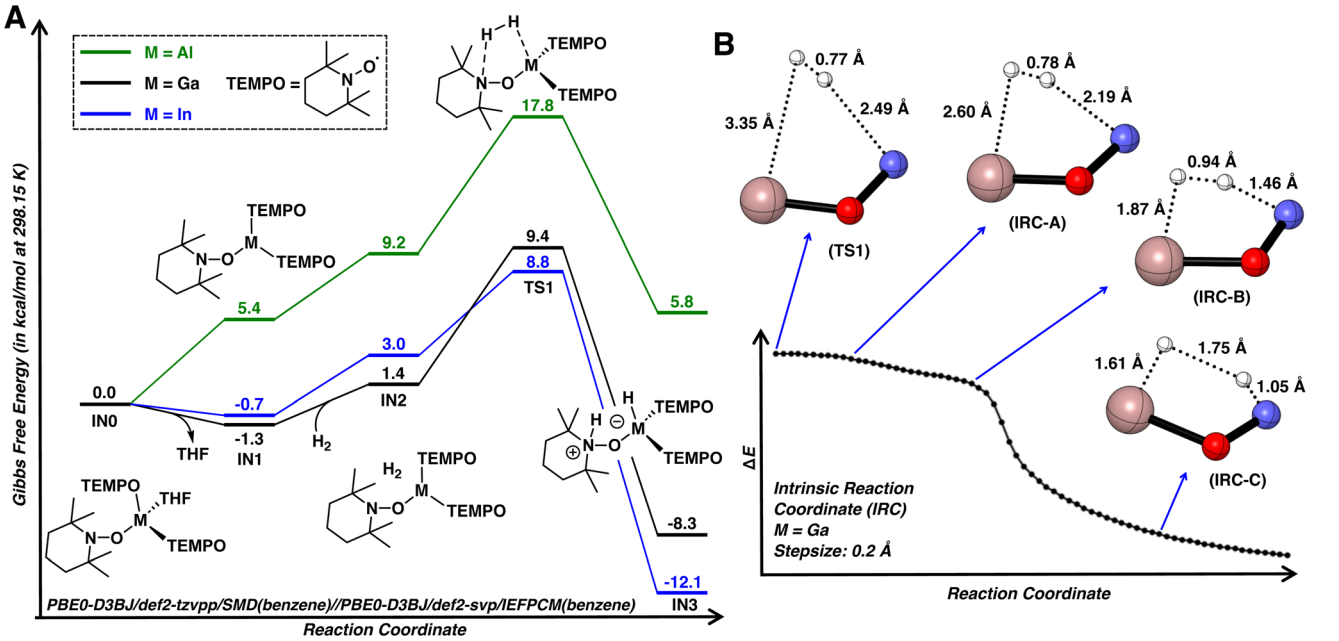

Fig. 5 (A) Computed reaction pathway for H_2 activation by complexes **1**·THF, **2**·THF, and **3**·THF. (B) Forward intrinsic reaction coordinate for **TS1** (M = Ga) and associated bond lengths of selected structures. Selected atoms were omitted for clarity. Color code: N, blue; O, red; Ga, salmon; H, white.

structural changes at the gallium atom and H–H bond (**IRC-A**). Upon reaching the Ga and N atoms (**IRC-B**), the H–H bond is rapidly elongated, resulting a quick decrease in energy until the dihydrogen is completely cleaved to form **IN3**. The concerted nature of H–H bond cleavage is consistent with previous computational studies on intramolecular frustrated Lewis pairs.[52]

Similar to **1**, complex **2** readily activates dihydrogen with a barrier of 9.5 kcal mol^{-1}, leading to a metastable indium hydride (Fig. 5A; see S.3.1.2† for a more detailed discussion on the subsequent formation of **5**). However, a significantly higher barrier of 17.8 kcal mol^{-1} was found for **3**, consistent with the relatively lower computed HIA for **3**. Although this barrier can be surmounted at room temperature, the resulting aluminum hydride is thermodynamically unfavorable by 5.8 kcal mol^{-1}, which precludes its isolation. Note that group 13 complexes of the form $[MH_2(TEMPO)quin]$ (M = Al, Ga; quin = quinuclidine) or $[MH(TEMPO)_2quin]$ (M = Al) were previously prepared *via* the oxidation of the corresponding quinuclidine bound metal hydrides with TEMPO.[16] The low temperature (*ca.* −50 °C) evolution of hydrogen at the onset of the reaction of quinuclidine bound metal hydrides with TEMPO suggests a thermodynamic driving force for the replacement of M–H bonds for M–TEMPO bonds in earlier group 13 metals.

Conclusion

The present work describes the facile heterolytic cleavage of H_2 by trivalent group 13 complexes with structurally affixed pendant amines, highlighting the utility of MLC in the context small molecule activation by complexes bearing a redox-innocent metal atom. This mode of activation is likely generalizable to other aminoxy–metal complexes and may have been inadvertently observed for $Zn(TEMPO)_2$.[53] Additionally, for trivalent indium, complete reduction to indium metal was observed and this pathway was leveraged in the synthesis of binary InSe. Notably, analogous chemical reactivity was not observed from bulk In metal, highlighting that low valent metal redox chemistry hitherto inaccessible may be exploited for the syntheses of materials through MLC. The established synthetic and reaction chemistry of aminoxyl radicals,[54–56] coupled with the simple synthesis of aminoxy–element complexes, provides a ripe opportunity for developing highly tunable systems for bond activation reactions.

Data availability

Crystallographic data are available from the Cambridge Structural Database under refcodes 2347342, 2347343, 2347344, 2347345, and 2347346. Full synthetic and computational details, including preparative procedures and spectroscopic data for characterization of compounds, are available in the ESI.†

Author contributions

M.-L. Y. Riu performed all experiments and prepared the manuscript and ESI.† DFT calculations were conducted by J.-R. Shan, K. N. Houk, and M.-L. Y. Riu. M. Nava directed the project and revised the manuscript. All authors have given approval to the final version of the manuscript.

© 2025 The Author(s). Published by the Royal Society of Chemistry

Open Access Article. Published on 22 2568. Downloaded on 10/8/2568 14:13:08. This article is licensed under a Creative Commons Attribution 3.0 Unported Licence.

Conflicts of interest

There are no conflicts to declare.

Acknowledgements

The authors acknowledge the startup fund from the University of California, Los Angeles (for M. N.), the financial support of the Jeffery and Helo Zink Endowed Professional Development Term Chair (for M. N.), the National Science Foundation (CHE-2153972 for K. N. H.), and computational resources from Expanse at SDSC through allocation CHE040014 from the Advanced Cyberinfrastructure Coordination Ecosystem: Services & Support (ACCESS) program (for K. N. H. and J.-R. S.). Molecular & Nano Archaeology (MNA) Laboratory at UCLA Materials Science Department are acknowledge for SEM use. Dr Tyler Kerr is acknowledged for his assistance with X-ray diffraction studies. George Wong is acknowledged for his assistance with elemental analysis. Prof. Peter Wolczanski and Dr David Gygi are acknowledged for helpful conversations.

References

1 J. R. Khusnutdinova and D. Milstein, *Angew. Chem., Int. Ed.*, 2015, **54**, 12236–12273.
2 M. D. Wodrich and X. Hu, *Nat. Rev. Chem*, 2017, **2**, 1–7.
3 L. Greb, F. Ebner, Y. Ginzburg and L. M. Sigmund, *Eur. J. Inorg. Chem.*, 2020, 3030–3047.
4 P. P. Power, *Nature*, 2010, **463**, 171–177.
5 R. L. Melen, *Science*, 2019, **363**, 479–484.
6 D. W. Stephan and G. Erker, *Angew. Chem., Int. Ed.*, 2015, **54**, 6400–6441.
7 A. J. I. Arduengo and C. A. Stewart, *Chem. Rev.*, 1994, **94**, 1215–1237.
8 J. M. Lipshultz, G. Li and A. T. Radosevich, *J. Am. Chem. Soc.*, 2021, **143**, 1699–1721.
9 S. Yadav, S. Saha and S. S. Sen, *ChemCatChem*, 2016, **8**, 486–501.
10 T. Chu and G. I. Nikonov, *Chem. Rev.*, 2018, **118**, 3608–3680.
11 E. R. M. Habraken, A. R. Jupp, M. B. Brands, M. Nieger, A. W. Ehlers and J. C. Slootweg, *Eur. J. Inorg. Chem.*, 2019, 2436–2442.
12 J. S. Scott, M. L. Maenaga, A. J. Woodside, V. W. Guo, A. R. Cheriel, M. R. Gau, P. R. Rablen and C. R. Graves, *Inorg. Chem.*, 2024, **63**, 4028–4038.
13 A. K. Kayser, P. T. Wolczanski, T. R. Cundari, M. M. Bollmeyer, K. M. Lancaster and S. N. MacMillan, *Chem. Commun.*, 2022, **58**, 9818–9821.
14 C. Lustig and N. W. Mitzel, *Angew. Chem., Int. Ed.*, 2001, **40**, 4390.
15 N. W. Mitzel, C. Lustig and M. Woski, *Dalton Trans.*, 2004, 397–401.
16 C. Jones and R. P. Rose, *New J. Chem.*, 2007, **31**, 1484–1487.
17 P. Bösing, A. Willner, T. Pape, A. Hepp and N. W. Mitzel, *Dalton Trans.*, 2008, 2549–2556.
18 P. Bösing, B. Neumann, H.-G. Stammler and N. W. Mitzel, *Z. Anorg. Allg. Chem.*, 2009, **635**, 2388–2390.
19 B. J. Hellmann, A. Mix, B. Neumann, H.-G. Stammler and N. W. Mitzel, *Dalton Trans.*, 2010, **39**, 7073–7079.
20 J. P. Dombrowski, G. R. Johnson, A. T. Bell and T. D. Tilley, *Dalton Trans.*, 2016, **45**, 11025–11034.
21 A. W. Apblett, A. C. Warren and A. R. Barron, *Can. J. Chem.*, 1992, **70**, 771–778.
22 A. J. Downs and C. R. Pulham, *Adv. Inorg. Chem.*, 1994, **41**, 171–232.
23 D. Isrow and B. Captain, *Inorg. Chem.*, 2011, **50**, 5864–5866.
24 J. A. B. Abdalla, I. M. Riddlestone, R. Tirfoin and S. Aldridge, *Angew. Chem., Int. Ed.*, 2015, **54**, 5098–5102.
25 W. Li, C. Li and Y. Lyu, *J. Catal.*, 2019, **373**, 1–12.
26 D. W. N. Wilson, J. Feld and J. M. Goicoechea, *Angew. Chem., Int. Ed.*, 2020, **59**, 20914–20918.
27 Z.-F. Zhang, M.-C. Yang and M.-D. Su, *Inorg. Chem.*, 2021, **60**, 15253–15269.
28 L. Wickemeyer, N. Aders, A. Mix, B. Neumann, H.-G. Stammler, J. J. Cabrera-Trujillo, I. Fernández and N. W. Mitzel, *Chem. Sci.*, 2022, **13**, 8088–8094.
29 M. Xu, J. Possart, A. E. Waked, J. Roy, W. Uhl and D. W. Stephan, *Philos. Trans. R. Soc., A*, 2017, **375**, 20170014.
30 A. J. Downs and C. R. Pulham, *Chem. Soc. Rev.*, 1994, **23**, 175–184.
31 C. Jones, *Chem. Commun.*, 2001, **22**, 2293–2298.
32 M. M. D. Roy, A. A. Omaña, A. S. S. Wilson, M. S. Hill, S. Aldridge and E. Rivard, *Chem. Rev.*, 2021, **121**, 12784–12965.
33 A. Wu, E. A. Mader, A. Datta, D. A. Hrovat, W. T. Borden and J. M. Mayer, *J. Am. Chem. Soc.*, 2009, **131**, 11985–11997.
34 N. W. Mitzel, U. Losehand, A. Wu, D. Cremer and D. W. H. Rankin, *J. Am. Chem. Soc.*, 2000, **122**, 4471–4482.
35 N. W. Mitzel, K. Vojinović, R. Fröhlich, T. Foerster, H. E. Robertson, K. B. Borisenko and D. W. H. Rankin, *J. Am. Chem. Soc.*, 2005, **127**, 13705–13713.
36 S. Alvarez, *Dalton Trans.*, 2013, **42**, 8617–8636.
37 P. Politzer and J. S. Murray, *Struct. Chem.*, 2021, **32**, 623–629.
38 P. N. Bartlett, D. Cook, C. H. K. de Groot, A. L. Hector, R. Huang, A. Jolleys, G. P. Kissling, W. Levason, S. J. Pearce and G. Reid, *RSC Adv.*, 2013, **3**, 15645–15654.
39 A. Bard, R. Parsons and J. Jordan, *Standard Potentials in Aqueous Solution*, CRC Press, 1985.
40 D. W. Boukhvalov, B. Gürbulak, S. Duman, L. Wang, A. Politano, L. S. Caputi, G. Chiarello and A. Cupolillo, *Nanomaterials*, 2017, **7**, 372.
41 H. Okamoto, *J. Phase Equilib. Diffus.*, 2004, **25**, 201.
42 C. De Blasi, G. Micocci, S. Mongelli and A. Tepore, *J. Cryst. Growth*, 1982, **57**, 482–486.
43 K. Çınar Demir, E. Demir, S. Yüksel and C. Coşkun, *Curr. Appl. Phys.*, 2019, **19**, 1404–1413.
44 E. K. Byrne, L. Parkanyi and K. H. Theopold, *Science*, 1988, **241**, 332–334.
45 P. Erdmann and L. Greb, *Angew. Chem., Int. Ed.*, 2022, **61**, e202114550.
46 M. O. Akram, J. R. Tidwell, J. L. Dutton and C. D. Martin, *Angew. Chem., Int. Ed.*, 2022, **61**, e202212073.
47 I. B. Sivaev and V. I. Bregadze, *Coord. Chem. Rev.*, 2014, **270–271**, 75–88.

© 2025 The Author(s). Published by the Royal Society of Chemistry

48 P. Erdmann and L. Greb, *ChemPhysChem*, 2021, **22**, 935–943.
49 G. C. Welch and D. W. Stephan, *J. Am. Chem. Soc.*, 2007, **129**, 1880–1881.
50 G. Ménard and D. W. Stephan, *Angew. Chem., Int. Ed.*, 2012, **51**, 8272–8275.
51 E. S. Wiedner, A. M. Appel, S. Raugei, W. J. Shaw and R. M. Bullock, *Chem. Rev.*, 2022, **122**, 12427–12474.
52 J. Daru, I. Bakó, A. Stirling and I. Pápai, *ACS Catal.*, 2019, **9**, 6049–6057.
53 P. Jochmann and D. W. Stephan, *Chem. Commun.*, 2014, **50**, 8395–8397.
54 L. B. Volodarsky, V. A. Reznikov and V. I. Ovcharenko, *Synthetic Chemistry of Stable Nitroxides*, CRC Press, Boca Raton, FL, 1994.
55 H. Karoui, F. L. Moigne, O. Ouari and P. Tordo, *Stable Radicals*, John Wiley & Sons, Ltd, 2010, ch. 5, pp. 173–229.
56 D. Leifert and A. Studer, *Chem. Rev.*, 2023, **123**, 10302–10380.

Open Access Article. Published on 22 2568. Downloaded on 10/8/2568 14:13:08.
This article is licensed under a Creative Commons Attribution 3.0 Unported Licence.

© 2025 The Author(s). Published by the Royal Society of Chemistry